Available online at www.sciencedirect.com
SCIENCE DIRECT®
International Journal of Thermal Sciences 42 (2003) 857–870
International Journal of Thermal Sciences
www.elsevier.com/locate/ijts

Designed porous media: Optimally nonuniform flow structures connecting one point with more points ☆

J.C. Ordonez [a], A. Bejan [a,*], R.S. Cherry [b]

[a] *Department of Mechanical Engineering and Materials Science, Duke University, Box 90300, Durham, NC 27708-0300, USA*
[b] *Idaho National Engineering and Environmental Laboratory, P.O. Box 1625, Idaho Falls, ID 83415-2203, USA*

Received 13 June 2002; accepted 19 November 2002

Abstract

This paper shows analytically and numerically how an originally uniform flow structure transforms itself into a nonuniform one when the objective is to minimize global flow losses. The flow connects one point (source, sink) to a number of points (sinks, sources) distributed uniformly over a two-dimensional domain. In the first part of the paper, the flow between neighboring points is modeled as fully developed through round tubes. It is shown that flow 'maldistribution' and the abandonment of symmetry are necessary for the development of flow structures with minimal resistance. The search for better flow structures can be accelerated: tubes that show a tendency of shrinking during the search can be assumed absent in future steps of structure optimization. In the second part of the paper, the flow medium is continuous and permeated by Darcy flow. The development of flow structures (channels) is modeled as a mechanism of erosion, where elements of the original medium are removed one by one, and are replaced with a more permeable medium. The elements selected for removal are identified based on two criteria: maximum pressure integrated over the element boundary, and maximum pressure gradient. The flow structures generated based on the pressure gradient criterion have consistently smaller flow resistances. As flow systems become smaller and more compact, the flow systems themselves become "designed porous media". These design optimization trends revealed are generally applicable in constructal design, i.e., where miniaturization, global performance, compactness and complexity rule the design.

Keywords: Constructal; Porous media; Dendritic; Trees; Topology; Geometry; Optimization

1. Flow maldistribution, or paths of least resistance

Many engineering applications call for the judicious distribution of a flowing fluid through a volume. This requirement stems from the need to maximize the global performance of the macroscopic system, and the thought that every volume element should function at the same (the highest) level of performance as any other volume element. For example, uniform distribution of flow rate is often a requirement in the design of banks of parallel tubes in heat exchangers (e.g., Fig. 1, top). One tube is thought to perform the same as its neighbor. This idea is attractive because it makes the design and its analytical description simple.

Thermal engineering is rich in examples of how the intended uniform distribution is difficult to maintain in practice. A stream that is forced to flow through the coarse porous structure formed by assemblies of ducts has a mind of its own. It permanently seeks paths of least resistance, and in this process the planned uniformity is threatened, or destroyed. In heat exchanger technology the result of this tendency is known as flow maldistribution. It is a bad, unwanted result. The same phenomenon is at work in other flow structures with multiple parallel streams, for example, in nuclear reactor cores, packed beds, volumetrically cooled electric windings and packages of electronics [1–9].

The classical view on the origin of flow maldistribution rests on a feedback mechanism associated with the clogging and widening of ducts. Clogging may be due to accumulation of scale on the duct surface, or the formation of gas bubbles and pockets of fluid with greater viscosity when the duct wall heats the stream. In the clogged duct the flow slows down, and this generally leads to an intensification of the mechanism that produces clogging. Larger flow rates have the effect of widening ducts with stretchable walls. This positive feedback pushes the clogged or widened ducts toward

☆ This work was supported by the Laboratory Directed Research and Development program at the INEEL, which is managed and operated by Bechtel BWXT Idaho Inc. under DOE Idaho Operations Office Contract DE-AC07-99ID13727.
* Corresponding author.

1290-0729/$ – see front matter
doi:10.1016/S1290-0729(03)00058-9

Nomenclature

A_p	tube cross-sectional area	m^2
d	pore length scale	m
D	tube diameter, Figs. 1–6	m
D	side of square erodable block, Fig. 7	m
k	thermal conductivity	$W{\cdot}m^{-1}{\cdot}K^{-1}$
K	permeability	m^2
L	length	m
$\dot{m}$	mass flow rate	$kg{\cdot}s^{-1}$
$\dot{m}''$	mass flow rate per unit area	$kg{\cdot}m^{-2}{\cdot}s^{-1}$
P	pressure	Pa
$q_{1,2}$	conduction heat currents	W
R	global flow resistance, dimensionless, Eq. (5)	
u, v	volume averaged velocity components, Eq. (14)	
V	volume	m^3
x, y	Cartesian coordinates	m

Greek symbols

β	constant, Eq. (20)	
ΔP	pressure difference	Pa
ΔT	temperature difference	K
μ	viscosity	$kg{\cdot}s^{-1}{\cdot}m^{-1}$
ν	kinematic viscosity	$m^2{\cdot}s^{-1}$
ρ	density	$kg{\cdot}m^{-3}$
ϕ	porosity	

Superscript

$\sim$	dimensionless variables, Eqs. (4) and (16)

Subscripts

0	reference permeability
1	low permeability
2	high permeability

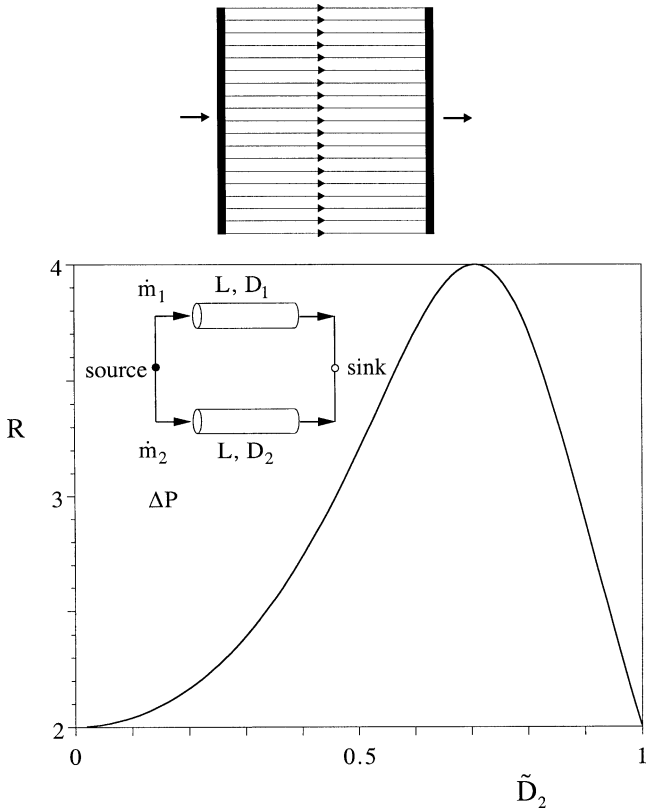

Fig. 1. Uniformly distributed flow through identical and parallel tubes (top), and the minimization of the flow resistance of a pair of tubes (bottom).

further clogging or widening, and toward more accentuated maldistribution.

In this paper we propose to look at the flow maldistribution phenomenon from the point of view of constructal theory, whereby the natural progress of flow structures is in the direction of maximizing access for the material that flows—minimum flow resistance, increasing flow complexity, and maximum spreading of flowing material [10]. The flow configuration is not specified a priori. It is the main unknown—the design. The configuration is free to change in the pursuit of a global objective subject to global constraints.

Fluid streams have a characteristic analogous to the economies of scale known in economics: the transportation cost per unit decreases when the goods are transported in larger and larger quantities. The analogy is this: larger streams flow more easily through correspondingly wider ducts. Said another way, two small streams flow more easily when they flow together through a single duct. The inside-out counterpart of this configuration exhibits the same behavior: two solid bodies traveling through a fluid encounter less drag when they travel together [10,11].

Geometric features (e.g., coalescence) generated by the search for less resistance endow the larger flow system with organization, structure, geometry, or topology. What is perceived as bad ("mal" distribution) because of the rigid assumption of flow uniformity, is in fact good from the point of view of minimizing all the internal flow resistances together, by balancing the streams against each other in such a way that the global resistance of the macroscopic and highly complex system is minimum. The emerging flow structure is heterogeneous, not parallel and uniform.

Additional functions such as heating, cooling and mass transfer can be designed into the optimally distributed flow system. To illustrate this additional step is not the objective of this paper. Recent publications illustrate convincingly the opportunity that comes from freeing the design of the uniform parallel flow assumption. Applications are emerging in chemical engineering [12], chemical and bioreactors [13–16] and electronics cooling [10,17]. In this paper we focus strictly on fluid flow, and on how an assumed uniform flow

structure morphs itself into a nonuniform one in which some ducts grow, others shrink, while others disappear completely.

2. Flow between two points

The simplest setting for illustrating this morphing process is the flow between one source and one sink. The law of optimization of flow access [10] requires straight ducts and circular flow cross-sections: we take these geometric features as first results, i.e., as starting point. In the lower part of Fig. 1 we seek to optimize the access between the two points by using two parallel round tubes of fixed length L and diameters D_1 and D_2. When the tubes are identical ($D_1 = D_2$), they may be viewed as two 'elemental volumes' of the system with prescribed uniform flow distribution (Fig. 1, top).

The pressure difference across the two-tube assembly is fixed, ΔP. Throughout this paper we assume that the flow is in the Hagen–Poiseuille regime, therefore we write.

$$\dot{m}_1 = \frac{\pi D_1^4 \Delta P}{128 \nu L} \tag{1}$$

$$\dot{m}_2 = \frac{\pi D_2^4 \Delta P}{128 \nu L} \tag{2}$$

We also assume that the space occupied by the tubes is constrained, $V_\mathrm{p} = (\pi/4) A_\mathrm{p} L$, where A_p represents the order of magnitude of the sum of tube cross-sectional areas,

$$A_\mathrm{p} = D_1^2 + D_2^2 \tag{3}$$

Mass conservation requires $\dot{m}_1 + \dot{m}_2 = 2\dot{m}$, where $\dot{m}$ is the flow rate through one tube when the distribution is uniform. Linear dimensions can be nondimensionalized by using $A_\mathrm{p}^{1/2}$ as scale,

$$\left(\widetilde{D}_1, \widetilde{D}_2\right) = (D_1, D_2)/A_\mathrm{p}^{1/2} \tag{4}$$

The objective is to minimize the flow resistance $\Delta P/(2\dot{m})$, or $\Delta P/\dot{m}$, which is represented in dimensionless terms by the group

$$R = \frac{\Delta P/\dot{m}}{128 \nu L/(\pi A_\mathrm{p}^2)} \tag{5}$$

The emphasis is on minimizing losses (fluid power), which is equivalent to minimizing pressure drops when flow rates are specified. The two features that vary (D_1, D_2) are related via constraint (3), such that the R formula that results from Eqs. (1)–(4) has only one free parameter, for example, $\widetilde{D}_2$:

$$R = \frac{2}{(1 - \widetilde{D}_2^2)^2 + \widetilde{D}_2^4} \tag{6}$$

The $\widetilde{D}_2$ range is $[0, 1]$. Fig. 1 shows that the flow resistance R is maximum when $\widetilde{D}_2 = 2^{-1/2}$, which represents the design with uniform flow distribution ($D_1 = D_2$, $\dot{m}_1 = \dot{m}_2$). This configuration is unstable if the natural tendency is for geometry to progress toward lower flow resistance. Lower resistances are available toward larger and smaller values of $\widetilde{D}_2$. The lowest ($R = 2$) occurs when one of the tubes disappears ($\widetilde{D}_2 = 0$, or $\widetilde{D}_1 = 0$). The total stream ($\dot{m}_1 + \dot{m}_2$) finds it much easier to flow through a fixed volume if that volume is configured as a single tube.

3. Flow between three corner points and one point in a square loop

More complex flows show the same behavior, although the resulting flow structure is more complex and tends to hide its origin. Consider four points in a square loop (Fig. 2, top), and assume that three (the black circles) are sources of equal flow rate ($\dot{m}$). The fourth is the sink that collects the total flow rate $3\dot{m}$. The four tubes that connect these points have the same length (L), but their diameters are different (D_1, D_2, D_3, D_4).

The objective is to minimize the global flow resistance $\Delta P/(3\dot{m})$, or $\Delta P/\dot{m}$, or the dimensionless resistance defined in Eq. (5), where ΔP is the pressure difference between the highest and the lowest pressures in the flow structure. The largest pressure difference ΔP is indicative of the correct scale of the pressure differences that drive the flow globally. Earlier constructal designs [10] have shown that by minimizing the largest potential difference one generates dendritic flow structures that are essentially the same as those generated by minimizing the potential difference averaged over all the points of the domain.

The tube volume constraint ($V_\mathrm{p} = \frac{\pi}{4} A_\mathrm{p} L$) is based on

$$A_\mathrm{p} = D_1^2 + D_2^2 + D_3^2 + D_4^2 \tag{7}$$

and the dimensionless diameters are $\widetilde{D}_i = D_i/A_\mathrm{p}^{1/2}$ ($i = 1, \ldots, 4$). Only three of these diameters are free to vary, for example, $\widetilde{D}_1$, $\widetilde{D}_2$, and $\widetilde{D}_3$. The question is how the 4-point system should be configured such that R is minimum. The analysis consists of writing continuity statements for flow rate ($\dot{m}_1 + \dot{m}_3 = 3\dot{m}$; $\dot{m}_1 - \dot{m}_2 = \dot{m}$; $\dot{m}_3 - \dot{m}_4 = \dot{m}$; $\dot{m}_4 + \dot{m}_2 = \dot{m}$) and pressure ($\Delta P_1 + \Delta P_2 = \Delta P$; $\Delta P_3 + \Delta P_4 = \Delta P$, where ΔP is the global pressure drop), assuming Hagen–Poiseuille flow,

$$\dot{m}_i = \frac{\pi D_i^4 \Delta P_i}{128 \nu L} \quad (i = 1, \ldots, 4) \tag{8}$$

and using Eq. (7) to eliminate D_4. The resulting expression for the overall resistance is

$$R = \left[3 - \frac{\widetilde{D}_1^4}{\widetilde{D}_1^4 + \widetilde{D}_2^4} - \frac{\widetilde{D}_3^4}{\widetilde{D}_3^4 + (1 - \widetilde{D}_1^2 - \widetilde{D}_2^2 - \widetilde{D}_3^2)^2}\right] \times \left[\frac{\widetilde{D}_1^4 \widetilde{D}_2^4}{\widetilde{D}_1^4 + \widetilde{D}_2^4} + \frac{\widetilde{D}_3^4 (1 - \widetilde{D}_1^2 - \widetilde{D}_2^2 - D_3^2)^2}{\widetilde{D}_3^4 + (1 - \widetilde{D}_1^2 - \widetilde{D}_2^2 - \widetilde{D}_3^2)^2}\right]^{-1} \tag{9}$$

The overall resistance is high ($R = 32$) when the flow structure is uniform ($\widetilde{D}_1 = \widetilde{D}_2 = \widetilde{D}_3 = \widetilde{D}_4 = 1/2$), as shown on the lower-left side of Fig. 2. The resistance drops dramatically ($R = 19.35$) when the structure is optimized

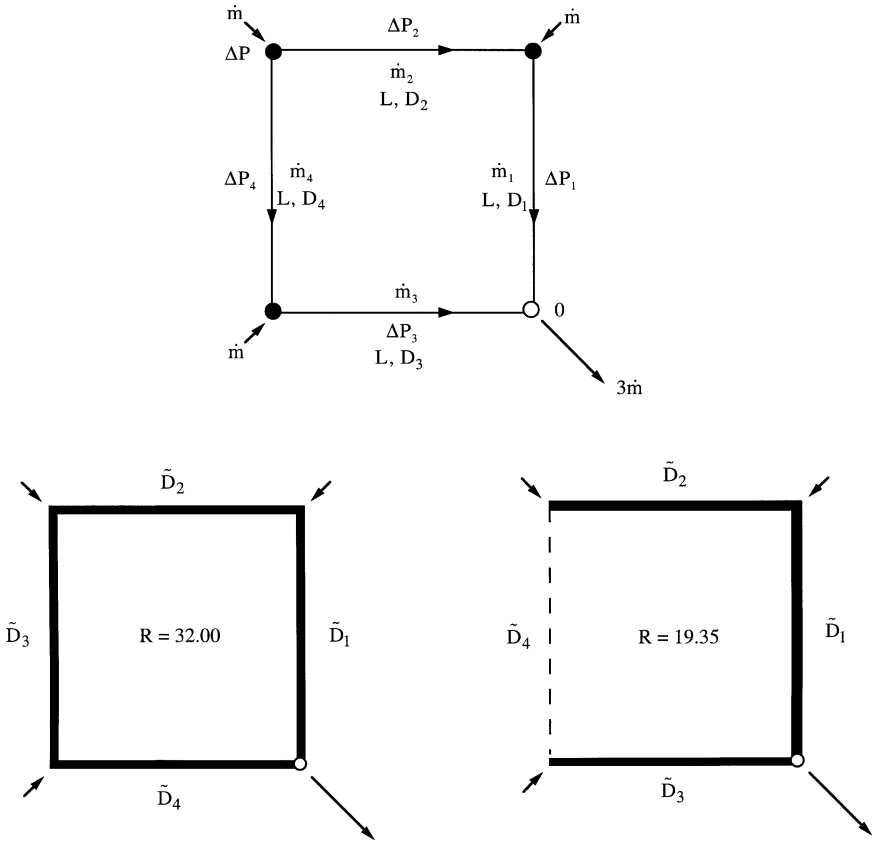

Fig. 2. Four tubes in a square connecting three sources with one sink. The uniform structure with tubes of the same size (left), and the nonuniform structure for minimum overall flow resistance (right).

with respect to its three degrees of freedom. This design is represented by

$$\widetilde{D}_1 = 0.651, \qquad \widetilde{D}_2 = 0.590$$
$$\widetilde{D}_3 = 0.477, \qquad \widetilde{D}_4 = 0 \tag{10}$$

The relative sizes of the optimized diameters are shown in the lower-right drawing of Fig. 2. Relative to the uniform structure where $\widetilde{D}_i = 1/2$, in the optimized structure the $\widetilde{D}_1$ and $\widetilde{D}_2$ tubes became wider, the $\widetilde{D}_3$ tube became narrower, and one of the tubes that do not touch the sink ($\widetilde{D}_4$ in Fig. 2) disappeared completely. In this configuration the source situated the farthest from the sink is connected by a single tube, not by two as in the uniform structure. Once again, postulated uniformity is a recipe for large flow resistance, and the tendency is for the structure to change into a nonuniform one.

A configuration that performs at a level between the two cases illustrated in Fig. 2 is the design that maintains symmetry with respect to the diagonal that passes through the source. In this case $\widetilde{D}_1 = \widetilde{D}_3$ and $\widetilde{D}_2 = \widetilde{D}_4$ serve as additional constraints, and there is only one degree of freedom: the ratio D_2/D_1, or D_3/D_4. The best design of this class is characterized by $\widetilde{D}_1 = 0.543$, $\widetilde{D}_2 = 0.452$ and $R = 29.13$. Compared with the R values listed under the two cases illustrated in Fig. 2, this level of performance ($R = 29.13$) shows that the resistance of the best design that preserves the square loop is considerably closer to the resistance of the other square-loop design that we considered ($R = 32$). In other words, the major improvement in performance is registered when symmetry is abandoned, so that tubes with free ends may form, and the loop itself may vanish.

4. More complex flow distribution networks

We find that loopless flow networks are progressively more efficient as we proceed toward more complex structures. In this section we document this course graphically, while omitting the analytical steps outlined for simple cases in the preceding two sections.

The top drawing of Fig. 3 shows a system of 12 tubes of the same size, which connect a central sink ($8\dot{m}$) to eight equal sources ($\dot{m}$) arranged on the perimeter of a square. This uniform structure has four loops. The maximum pressure difference occurs between the center (the source) and one of the corners of the large square. Note that this source-sink arrangement is not the same as joining together four of the square constructs studied in Fig. 2.

The structure can be optimized by selecting three of the tube diameters, because the fourth tube size results from the tube volume constraint

$$A_p = 2D_1^2 + 4D_2^2 + 2D_3^2 + 4D_4^2 \tag{11}$$

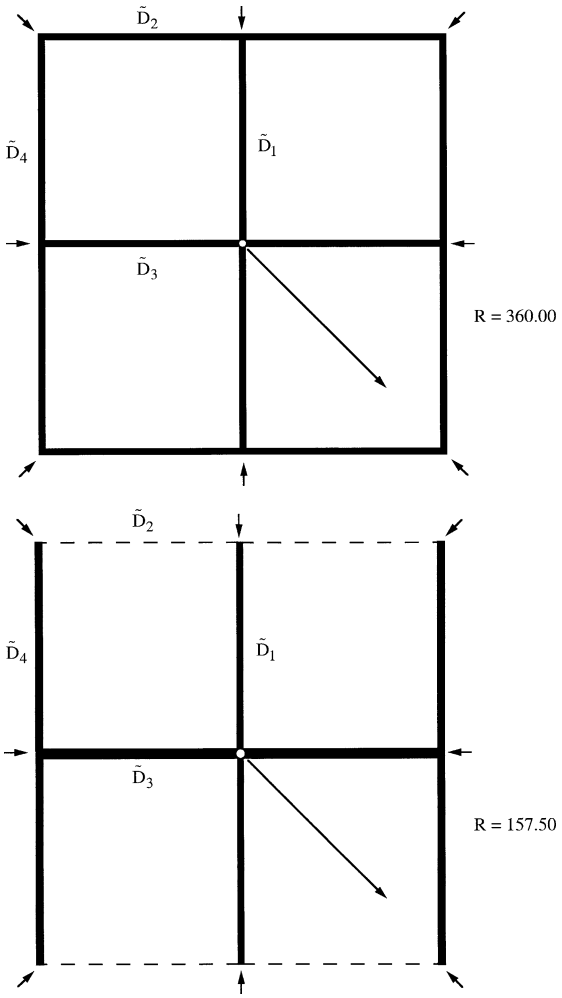

Fig. 3. Flow structure connecting one central sink with eight sources in a square. The uniform structure with tubes of the same size (top), and the nonuniform structure for minimum overall flow resistance (bottom).

In the uniform structure the dimensionless diameters ($\widetilde{D}_i = D_i/A_p^{1/2}$) are all equal to $12^{-1/2} = 0.289$, and the resistance (4) is $R = 360$. When R is minimized with respect to the three degrees of freedom, the structure acquires the features sketched in the lower frame of Fig. 3, where

$$\widetilde{D}_1 = 0.282, \qquad \widetilde{D}_2 = 0, \qquad \widetilde{D}_3 = 0.445, \qquad \widetilde{D}_4 = 0.333 \tag{12}$$

The four square loops have disappeared, and the overall resistance has dropped to less than half of the original value, $R = 157.5$.

An even more complex flow structure is shown in Fig. 4. Eight sources of equal flow rate ($\dot{m}$) are connected in a square grid pattern to one sink ($8\dot{m}$), which is situated in the lower-right corner. Recall that the structures of Figs. 1–3 were optimized by finding an expression for the dimensionless pressure drop R in terms of the unknown diameters, and by minimizing R. The minimization was performed by function evaluation in nested loops. That procedure worked well because there were only a few degrees of freedom.

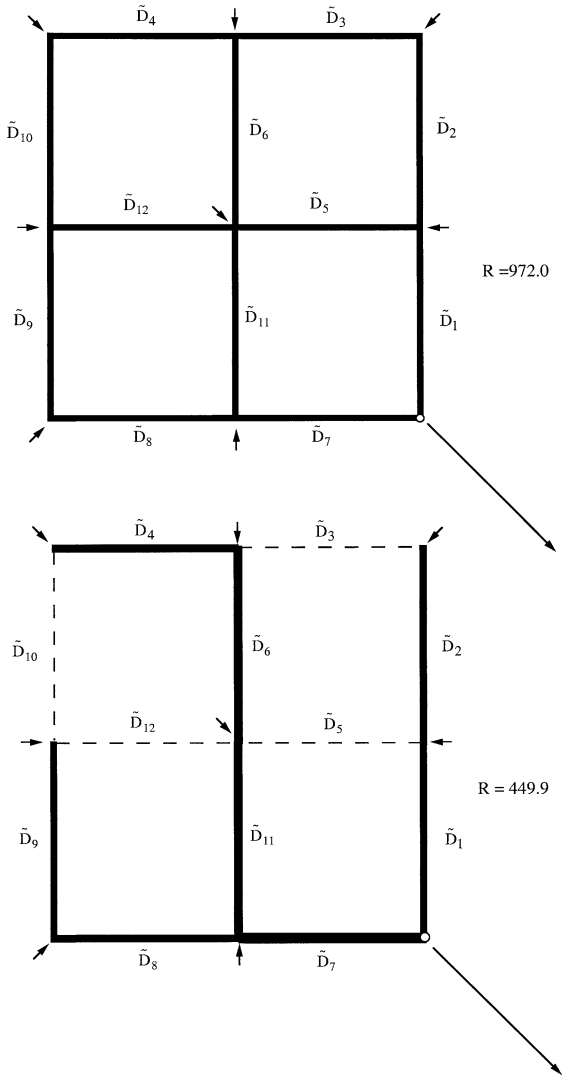

Fig. 4. Flow structure connecting eight sources with one corner sink. The uniform structure with tubes of the same size (top), and the nonuniform structure for minimum overall flow resistance (bottom).

The flow architecture of Fig. 4 has 12 degrees of freedom. Instead of developing an analytical expression for R, we found R by solving numerically the system of equations relating the mass flow rates to the pressure drops. Next, we performed the optimization of the structure by using a pseudo-random generator to generate values for the tube diameters that satisfy the total volume constraint A_p. We solved the system of equations for each set of diameters, and calculated R. We then compared the newly calculated R value with the smallest R calculated previously, and, if appropriate, we updated the smallest R value. In this methodology we know in advance that we will not find the optimal configuration (the one for which R is the absolute minimum), but we expect to find a configuration, or several configurations, the performance of which is close to the absolute best.

First, we tested this random-search procedure by applying it to the simpler flow structure of Fig. 3, eight sources

Table 1
Optimization results for the flow structure of Fig. 3

	Nested loops	Random search
$R_{\min}$	157.50	158.25
$\widetilde{D}_1$	0.2824	0.2837
$\widetilde{D}_2$	0	0.0122
$\widetilde{D}_3$	0.4453	0.4476
$\widetilde{D}_4$	0.3331	0.3308

with one central sink, for which we know the optimal configuration. The results obtained after 50 000 steps are listed in the last column of Table 1. The first column (nested loops) represents the results of the minimization of the analytical expression for R, namely Eq. (12) and the structure drawn in the lower part of Fig. 3. The step-by-step evolution of the random search is presented in the upper frame of Fig. 5, where the number of improvements on the abscissa represents the number of new configurations that perform better (at a lower R) than the starting configuration with all diameters equal ($R = 360$) as the search progresses. Table 1 shows that the random search leads to a flow structure and level of performance that approach very closely the results obtained with the minimization of the analytical expression.

Next, we applied the random search method to the optimization of the more complex structure of Fig. 4. We performed five searches consisting of 5×106 steps each. Each new search is based on a different state (seeds) for the pseudo-random generator, to ensure that a different set of diameter values is generated. The evolution of R is reported for each search in the lower part of Fig. 5. The lowest R value obtained in all five searches was 510.89, which corresponds to the diameters:

$$\begin{aligned}
&\widetilde{D}_1 = 0.3985, \quad \widetilde{D}_5 = 0.2647, \quad \widetilde{D}_9 = 0.3166\\
&\widetilde{D}_2 = 0.3942, \quad \widetilde{D}_6 = 0.1059, \quad \widetilde{D}_{10} = 0.0752\\
&\widetilde{D}_3 = 0.3592, \quad \widetilde{D}_7 = 0.3903, \quad \widetilde{D}_{11} = 0.0438\\
&\widetilde{D}_4 = 0.3468, \quad \widetilde{D}_8 = 0.3047, \quad \widetilde{D}_{12} = 0.0477
\end{aligned} \tag{13}$$

We performed additional computations to test the robustness of the results, and to try other configurations that are intuitively plausible, i.e., competitive relative to the configurations generated by the random search method. Table 2 summarizes these results. The first column shows the results of random search. In case 2 we used the results of the random search (first column), but imposed $\widetilde{D}_{11} = 0$ and increased $\widetilde{D}_1$ in order to satisfy the total volume constraint. In case 3 we switched the values of $\widetilde{D}_{11}$ and $\widetilde{D}_{12}$. In case 4 we set $\widetilde{D}_{10} = 0$ and increased $\widetilde{D}_1$ to satisfy the volume constraint.

The $R_{\min}$ values listed at the top of Table 2 show that these modifications (cases 2–4) produced only minor improvements in global performance. This supports the observation [10] that when the optimized structure becomes more complex, details such as the value assigned to $\widetilde{D}_{11}$ do not affect significantly the level of global performance. Optimized flow structures may not be identical in every detail, but each performs near the optimal level, and each resembles a tree.

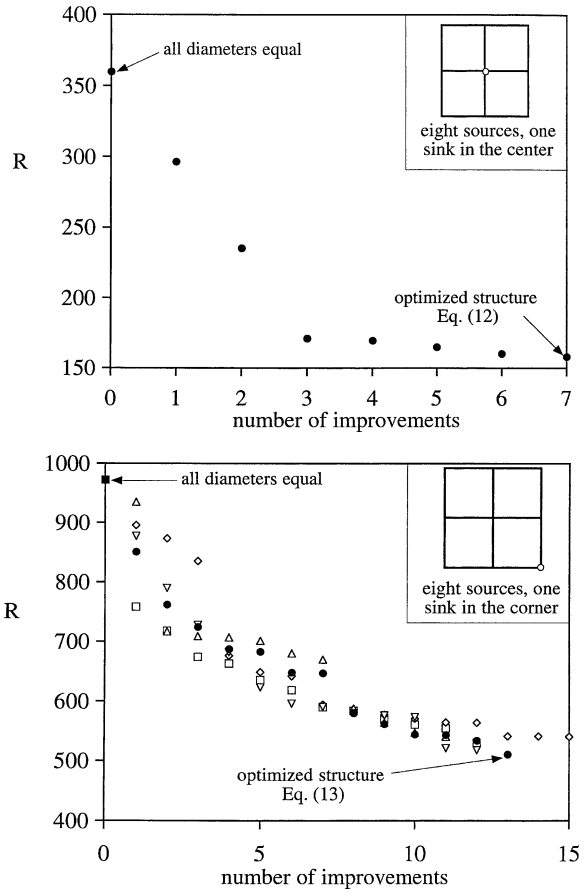

Fig. 5. Evolution of the random-search results for the structure with eight sources and one central sink (Fig. 3), and for the structure with eight sources and one corner sink (Fig. 4).

Another way to search for a flow structure better than cases 2–4, is to adopt the modifications from the start (e.g., set $\widetilde{D}_{10} = 0$), and to search for the remaining diameters. We considered six additional cases, which are reported in Table 3. In each case we performed five random-searches with 5×106 steps each.

The results for the case with $\widetilde{D}_{10} = 0$ are listed in the first column of Table 3. The overall resistance ($R = 481.14$) is lower than in all the tries summarized in Table 2, therefore we continued on this course and assumed that two tubes are absent, $\widetilde{D}_{10} = \widetilde{D}_6 = 0$. The results of the random search are listed under case 2 in Table 3, which also shows that the global resistance has decreased.

Case 1 of Table 3 also shows that $\widetilde{D}_{12}$ tends to disappear. In case 3 we assumed that $\widetilde{D}_{12}$ is absent, this in addition to setting $\widetilde{D}_{10} = 0$, and we registered an even smaller R value. In conclusion, the decision to assume away the tube that shows tendency of disappearing provides a shortcut toward lower resistances.

Cases 2 and 3 show that $\widetilde{D}_5$ is considerably smaller than the other diameters, which means that $\widetilde{D}_5$ tends to disappear. We started with this assumption in case 4, and repeated the

Table 2
Optimization results for the flow structure of Fig. 4

	Random search	Case 2	Case 3	Case 4
$R_{\min}$	510.8924	506.3647	510.9772	497.9279
$\widetilde{D}_1$	0.3985	0.4009	0.3985	0.4055
$\widetilde{D}_2$	0.3942	0.3942	0.3942	0.3942
$\widetilde{D}_3$	0.3592	0.3592	0.3592	0.3592
$\widetilde{D}_4$	0.3468	0.3468	0.3468	0.3468
$\widetilde{D}_5$	0.2647	0.2647	0.2647	0.2647
$\widetilde{D}_6$	0.1059	0.1059	0.1059	0.1059
$\widetilde{D}_7$	0.3903	0.3903	0.3903	0.3903
$\widetilde{D}_8$	0.3047	0.3047	0.3047	0.3047
$\widetilde{D}_9$	0.3166	0.3166	0.3166	0.3166
$\widetilde{D}_{10}$	0.0752	0.0752	0.0752	0
$\widetilde{D}_{11}$	0.0438	0	0.0477	0.0438
$\widetilde{D}_{12}$	0.0477	0.0477	0.0438	0.0477

random search by setting $\widetilde{D}_5 = \widetilde{D}_6 = \widetilde{D}_{10} = 0$ from the start. In this way, we obtained a lower global R value. Next, in case 5, we added $\widetilde{D}_5$ to the list of vanishing tubes, and the global resistance decreased even further.

Case 5 on Table 3 identifies $\widetilde{D}_3$ as the next and last candidate to disappear. This is the last candidate because if more than four tubes disappear then there will be one source that will not be connected to the sink. Case 6 shows the results obtained by assuming $\widetilde{D}_3 = \widetilde{D}_5 = \widetilde{D}_{10} = \widetilde{D}_{12} = 0$. The global resistance has decreased to 449.85, which is the lowest level. This structure is shown in the lower part of Fig. 4. The uniform structure shown in the upper figure is characterized by $\widetilde{D}_i = 12^{-1/2} = 0.289$ ($i = 1, 2, 3, \ldots, 12$) and $R = 972$. The overall flow resistance drops by 53.7 percent in going from the top structure to the bottom structure of Fig. 4.

The most complex flow structure that we have optimized by random search is shown in Fig. 6, where 24 equal sources are connected to one central sink. This structure must be optimized as a new case, because it cannot be generated by splicing together four of the structures optimized in Fig. 4. The upper drawing shows the uniform grid, where $R = 14\,400$ and $\widetilde{D}_i = (40)^{-1/2} = 0.1581$ ($i = 1, 2, 3, \ldots, 40$). The tube volume constraint is $A_p = 2(D_1^2 + D_2^2 + D_7^2 + D_8^2) + 4(D_3^2 + D_4^2 + D_5^2 + D_6^2 + D_9^2 + D_{10}^2 + D_{11}^2 + D_{12}^2) =$ constant. Following the same route and number of searches used in the optimization of the structure of Fig. 4 (namely, five searches per case, with 5×10^6 steps each), we started with all the ducts present, and found a configuration with $R = 6\,848.8$. In this configuration $\widetilde{D}_{10}$ was the smallest diameter. Next, we set $\widetilde{D}_{10} = 0$ from the beginning, and found $R = 6\,054.7$ with $\widetilde{D}_6$ as the smallest (non-zero) diameter. Next, by setting $\widetilde{D}_6 = \widetilde{D}_{10} = 0$ we obtained $R = 5\,494.2$ with $\widetilde{D}_{12}$ as smallest diameter. Next, after assuming, $\widetilde{D}_6 = \widetilde{D}_{10} = \widetilde{D}_{12} = 0$ we found $R = 4\,808.0$ with $\widetilde{D}_{11}$ as the smallest diameter. Finally, for $\widetilde{D}_6 = \widetilde{D}_{10} = \widetilde{D}_{11} = \widetilde{D}_{12} = 0$ the overall flow resistance dropped to $R = 4322.5$. This optimized structure is shown in the lower part of Fig. 6. The overall flow resistance dropped by 70 percent relative to the resistance of the structure on the top of Fig. 6.

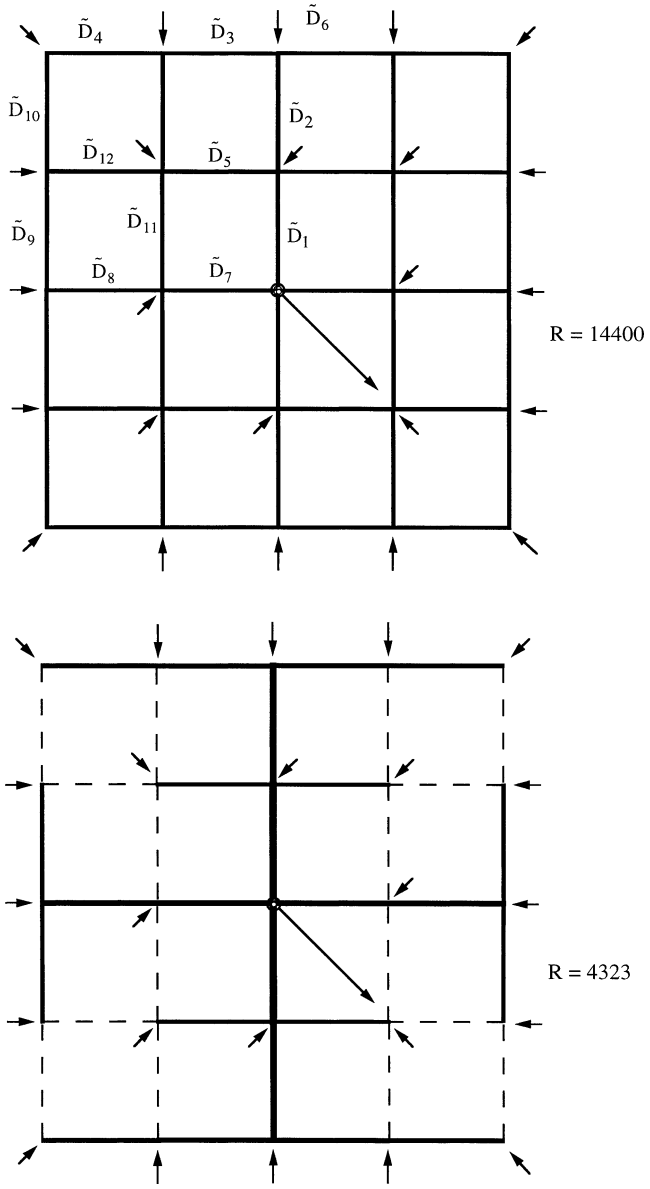

Fig. 6. Flow structure connecting 24 sources with one central sink. The uniform structure (top), and the nonuniform structure for minimum overall flow resistance (bottom).

Table 3
Optimization results for the structure of Fig. 4; tubes that show a tendency to disappear were assumed absent at the start of the numerical search for flow structures with lower resistance

	Case 1	Case 2	Case 3	Case 4	Case 5	Case 6
$R_{\min}$	481.1378	477.6312	474.8464	470.6260	467.6999	449.8539
$\widetilde{D}_1$	0.4043	0.4058	0.3887	0.4087	0.3449	0.3041
$\widetilde{D}_2$	0.4151	0.3994	0.4153	0.3867	0.2705	0.3134
$\widetilde{D}_3$	0.3616	0.3906	0.3549	0.3707	0.0589	0
$\widetilde{D}_4$	0.3386	0.2983	0.3423	0.3248	0.3294	0.3505
$\widetilde{D}_5$	0.2715	0.0041	0.0192	0	0	0
$\widetilde{D}_6$	0.0360	0	0.0811	0	0.3616	0.3753
$\widetilde{D}_7$	0.3836	0.3920	0.4123	0.3665	0.4310	0.4561
$\widetilde{D}_8$	0.3117	0.2499	0.3401	0.2560	0.3303	0.3286
$\widetilde{D}_9$	0.3082	0.1577	0.2781	0.1195	0.2996	0.2921
$\widetilde{D}_{10}$	0	0	0	0	0	0
$\widetilde{D}_{11}$	0.0565	0.3228	0.2517	0.3669	0.4248	0.3798
$\widetilde{D}_{12}$	0.0363	0.2984	0	0.3004	0	0

5. Erodable porous medium

The next step toward more complex flow structures is to consider the flow between an infinite number of identical sources and one sink. We assume that the sources are distributed uniformly over a two-dimensional domain (A), and their constant flow rate per unit area is $\dot{m}''$ [kg·m^{-2}·s^{-1}]. The entire stream generated over this domain escapes through one point sink, e.g., the lower-left corner of the square domain shown in Fig. 7. In place of all the tubes with Hagen–Poiseuille flow used in the preceding flow structure, here we assume seepage flow in the Darcy regime, in a generally nonuniform porous medium,

$$u = -\frac{K}{\mu}\frac{\partial P}{\partial x}, \qquad v = -\frac{K}{\mu}\frac{\partial P}{\partial y} \tag{14}$$

where (u, v) are the volume-averaged velocity components, and K is the local permeability of the medium. The conservation of mass requires

$$\frac{\partial u}{\partial x} + \frac{\partial v}{\partial y} = \frac{\dot{m}''}{\rho D} \tag{15}$$

The permeability K is in general not uniform. The flow erodes the medium in order to create for itself paths of reduced resistance. These paths are modeled as regions with increased permeability. The original (background) permeability of the medium that has not been eroded is lower than the permeability of the eroded regions. Erosion is modeled by dividing the domain into a large number of elemental blocks of length scale D, and by assuming that the flow removes (pushes out of the way) certain blocks. Eq. (15) can be nondimensionalized using D as length scale,

$$(\tilde{x}, \tilde{y}) = \frac{(x, y)}{D}, \qquad \widetilde{P} = \frac{P\rho K_0}{\dot{m}''\mu D} \tag{16}$$

where P is the pressure in excess of the pressure at the point sink, and K_0 is a reference permeability. Eq. (15) becomes

$$\frac{\partial}{\partial x}\left(\frac{K}{K_0}\frac{\partial \widetilde{P}}{\partial \tilde{x}}\right) + \frac{\partial}{\partial y}\left(\frac{K}{K_0}\frac{\partial \widetilde{P}}{\partial \tilde{y}}\right) + 1 = 0 \tag{17}$$

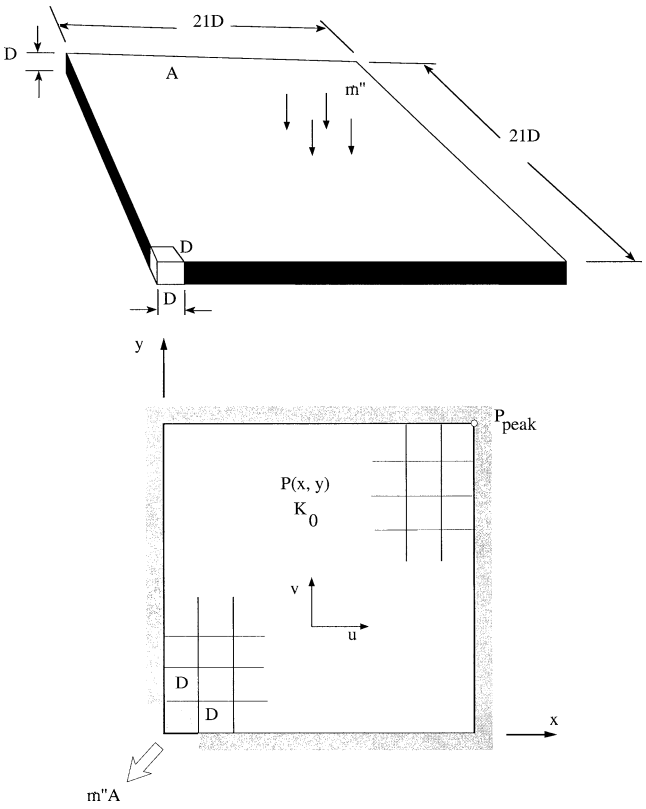

Fig. 7. Porous domain with mass flow rate generation at every point, and one sink in the lower-left corner.

Instead of the total tube volume constraint invoked in the preceding optimizations, here we assume that the void volume is fixed. The reference case is the original medium of permeability K_0 and uniform porosity ϕ_0. The corresponding void volume $\phi_0 V$ is fixed. This case is analogous to the uniform flow structures with tube diameters of only one size (e.g., Fig. 4, top). Instead of searching for the optimal distribution of tube diameters, now we search for the redistribution of void space such that the overall resistance decreases. The overall resistance is proportional to the largest pressure drop over the domain, namely $P_{\text{peak}} - 0$,

where P_{peak} is the pressure at the point with the highest pressure. This is analogous to the treatment of the flow structures of Figs. 2–4 and 6, where the highest pressure occurred at the source situated the farthest from the sink. The dimensionless peak pressure drop, which plays the role of the resistance R of the preceding flow structures, is

$$\widetilde{P}_{\text{peak}} = \frac{P_{\text{peak}} \rho K_0}{\dot{m}'' \mu D} \tag{18}$$

For simplicity, we assume that the void volume V is distributed over regions of only two types:

(1) Low permeability $K_1 < K_0$, porosity ϕ_1, volume V_1, void volume $\phi_1 V_1$.
(2) High permeability $K_2 > K_0$, porosity ϕ_2, volume V_2, void volume $\phi_2 V_2$.

The total volume occupied by the porous domain is fixed, $V = V_1 + V_2$. The total void volume is also fixed, $\phi_1 V_1 + \phi_2 V_2 = \phi_0 V$, or

$$\frac{\phi_1}{\phi_0}\frac{V_1}{V} + \frac{\phi_2}{\phi_0}\frac{V_2}{V} = 1 \tag{19}$$

Next, we assume Kozeny's relation between permeabilities and porosities

$$K_{0,1,2} = \frac{d^2 \phi_{0,1,2}^3}{\beta(1-\phi_{0,1,2})^2} \tag{20}$$

where β is a constant of order 10^2, and d is the pore (or particle) length scale. The permeability ratio K/K_0 appearing in Eq. (17) stands for K_1/K_0 or K_2/K_0, depending on the flow region. Such ratios are related to the respective porosities via Eq. (20),

$$\frac{K_{1,2}}{K_0} = \left(\frac{\phi_{1,2}}{\phi_0}\right)^3 \left(\frac{1-\phi_0}{1-\phi_{1,2}}\right)^2 \tag{21}$$

Numerical flow simulations were performed over a square domain made up of 21×21 elemental squares of side D, Fig. 7. An interesting question is how sensitive the numerical results will be to the number of elemental blocks used to discretize the domain. This is a good direction to explore in the future. The assumed reference porosity was $\phi_0 = 0.4$. We chose this value because it is representative of the range of sands and soils. The value of the corresponding permeability K_0 is not required for the calculations, but it could be estimated from Eq. (2) based on information regarding the pore length scale. The pressure distribution in the reference case is shown in Fig. 8. The peak pressure occurs in the upper-right corner, $\widetilde{P}_{\text{peak}} = 850.78$.

To study the question of how the nonuniform distribution of structure (porosity, permeability) can be used to lower the overall resistance to flow, we considered the case where the low- and high-permeability domains are characterized by $K_1/K_0 = 0.9$ and $K_2/K_0 = 10$. The corresponding porosity ratios are determined from Eq. (21), namely, $\phi_1/\phi_0 = 0.976$ and $\phi_2/\phi_0 = 1.568$. The volume ratios in this case are

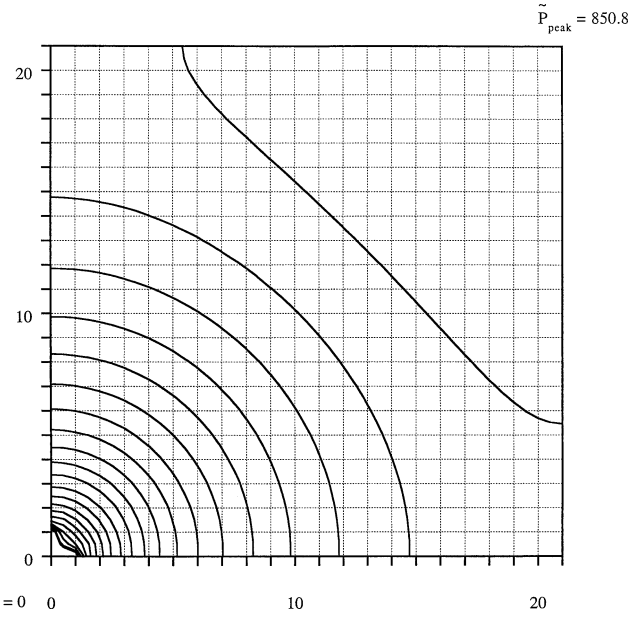

Fig. 8. The pressure distribution in the reference case where the permeability and porosity are uniform.

$V_1/V = 0.959$ and $V_2/V = 0.041$, meaning that out of the 21×21 elements, region 1 occupies 423 elements and region 2 occupies 18 elements.

Fig. 9 (case A) shows a configuration where region 2 is centered around the sink. The overall resistance is $\widetilde{P}_{\text{peak}} = 425.8$, which is almost half of the resistance in the reference case. Clearly, the redistribution of the voids has a large impact on the global resistance of the flow structure. The region with much higher permeability is located near the sink, that is, in the region where flow velocities are the highest. High velocities are also the cause of erosion in real porous media, and so the comparison of Fig. 8 and case A of Fig. 9 suggests that a structure generating mechanism such as erosion can have a great impact on lowering the global resistance.

The step taken in going from Figs. 8 and 9 (case A) is analogous to going from a uniform grid of tubes (e.g., Fig. 4, top) to a grid with two tube sizes, and placing the wider tubes near the point sink. Review Figs. 2–4 and 6, and note that in the optimized flow structures the tubes that touch the point sink are the widest. The question that remains is whether the concentration of high-permeability elements depicted in case A of Fig. 9 represents the optimal flow structure.

We pursued this question in cases B to E of Fig. 9, where the objective was to discover flow structures that evolve toward lower resistance. Five competing structures were compared. In case B, we removed at each step the element that had the highest pressure averaged over its surface and shared at least one face with the eroded (K_2) region. The first element was the one touching the sink. For the second element, we had a choice between the element immediately to the right of the first, and the one immediately above, both with the same value of averaged pressure. In case B, we

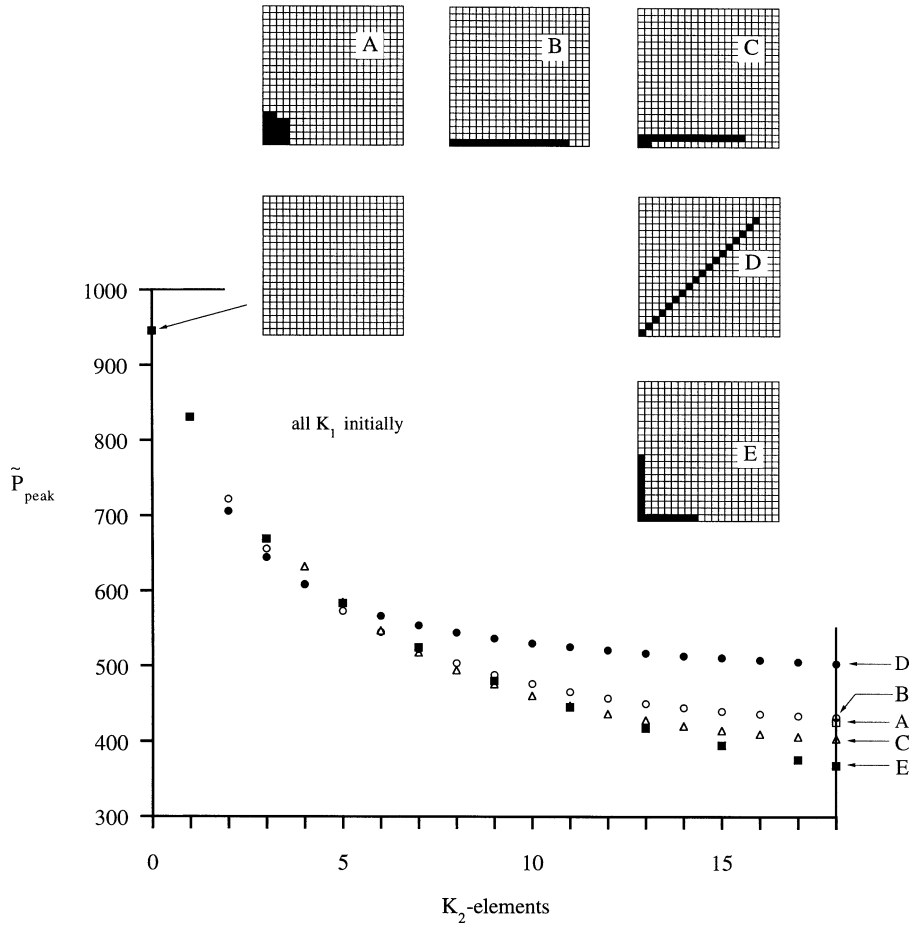

Fig. 9. Five scenarios showing the monotonic decrease in global resistance as finger-shaped regions of high permeability develop step by step.

wanted to remove one element at a time: we removed the one on the right, and continued the removal process. The figure shows that the overall resistance decreases at every step, and reaches 432.5 when 18 elements are removed.

Case C is based on a strategy that combines the strategies used in cases A and B. We started the erosion process by removing the four elements that are closest to the sink. The process was then continued by using the same strategy as for case B. The end result is that after the removal of all 18 elements the overall resistance dropped to a level lower than in cases A and B, namely $\widetilde{P}_{\text{peak}} = 403.31$.

Case D started with the removal of the element touching the sink, and continued with identifying and removing the next element that has the highest pressure averaged over its surface. We required that each such element touches (at one point) the existing K_2 region. In other words, unlike in cases B and C, the removed element did not have to share a face with the K_2 region. We found that the overall resistance decreases more slowly than in the preceding cases, reaching $\widetilde{P}_{\text{peak}} = 503.54$ after the removal of all 18 elements.

Case E is the result of starting the process as in case B, but removing the element (or elements) that have the highest pressure averaged over its surface and share a face with the K_2 region. The first removed element is the one that touches the sink. The next elements come in pairs. For example, in the second step we removed the elements situated to the right and above the first removed element. In this way the flow structure grows as two fingers, and the overall resistance drops to the lowest level, $\widetilde{P}_{\text{peak}} = 367.72$.

Scenarios B–E of Fig. 9 were all based on a pressure removal criterion. The element selected for removal was the one with the highest pressure integrated over its square boundary. An alternative is to seek the element with the maximum pressure gradient. This criterion is more realistic because the pressure gradient is proportional to (and balanced by) the cohesive stresses that connect the element to its neighbors, and keep the element in place.

This alternative was pursued for cases B to E of Fig. 9. The only change introduced is that instead of looking at elements with the highest averaged pressure, we searched for the element with the highest pressure gradient. The numerical experiments for cases B, C and D are reported in Fig. 10. In the top frame we show the evolution of the overall flow resistance in cases B and D. The overall flow resistance is considerably lower than in the corresponding structures based on the pressure removal criterion. The B and D structures obtained based on the pressure gradient criterion are the same, i.e., there is no difference when

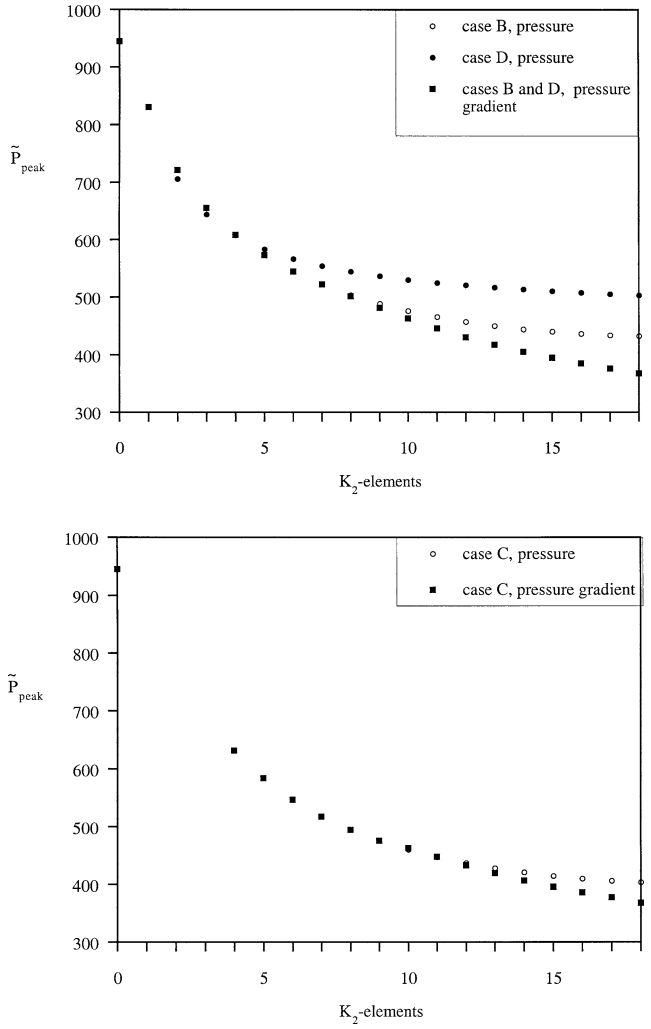

Fig. 10. The development of eroded flow structures based on the maximum pressure gradient criterion, and comparison with the flow resistance of structures based on the maximum pressure criterion.

removing one element at a time, using the highest pressure gradient criterion, if we choose from the elements that share a face with the K_2 region or those that touch it.

The lower frame of Fig. 10 shows the same comparison for case C. The identification and removal of the "most stressed" elements leads to eroded structures that have consistently lower flow resistances. The E structure obtained based on the pressure gradient criterion is the same as the E structure obtained based on the pressure criterion.

The generated structures and the removal sequences for cases B to E are reported in Fig. 11. The structures on the left are based on the pressure criterion, and those on the right are based on the pressure gradient. It is interesting to see that in the case of the pressure gradient criterion, which resulted in structures with lower resistances (Fig. 10), fingers appear and the structures look like the one obtained for case E based on the pressure criterion. The latter had the lower resistance in Fig. 9.

6. Optimal permeability

To summarize the porous medium model developed in Section 5, we started with a volume V filled with a reference (homogeneous) porous medium of permeability K_0 and porosity ϕ_0. The total void space $\phi_0 V$ is fixed, and is distributed uniformly through V. We then considered the construction of a combination of two flow regions inside V, with the objective of minimizing the overall flow resistance. Region 1 has the low permeability K_1 ($< K_0$), volume V_1, and porosity ϕ_1, while region 2 has the high permeability K_2 ($> K_0$), volume V_2, and porosity ϕ_2. The total volume and total void volume are fixed and equal to the reference values, $V_1 + V_2 = V$ and $\phi_1 V_1 + \phi_2 V_2 = \phi_0 V_0$.

In Section 5 we fixed the two permeabilities ($K_1/K_0 = 0.9$, $K_2/K_0 = 10$), and showed that it is important how V_1 and V_2 are distributed through V. The overall resistance is minimized by allowing V_2 to grow as fingers surrounded by V_1 (Fig. 9). In this section, we relax the K_2/K_0 constraint, and ask whether the high permeability can also be selected so that the overall flow resistance is minimized.

It can be shown that the total volume (V) and total void volume ($\phi_0 V$) constraints can be used to obtain

$$\frac{V_1}{V} = \frac{\phi_2 - \phi_0}{\phi_2 - \phi_1} \tag{22}$$

$$\frac{V_2}{V} = \frac{\phi_0 - \phi_1}{\phi_2 - \phi_1} \tag{23}$$

The lower limit of the high permeability is $K_2/K_0 = 1$. In this case $\phi_2 = \phi_0$ and $V_1 = 0$, and all the blocks that fill V are of type 2. We showed in Fig. 8 that in this limit $\widetilde{P}_{\text{peak}} = 850.78$ when $\phi_0 = 0.4$.

In the opposite extreme ($K_2/K_0 \to \infty$), ϕ_2 approaches 1, and V_1/V and V_2/V are bounded because $\phi_2 \leqslant 1$:

$$\frac{V_1}{V} \leqslant \frac{\phi_0 - 1}{\phi_1 - 1} \tag{24}$$

$$\frac{V_2}{V} \geqslant \frac{\phi_1 - \phi_0}{\phi_1 - 1} \tag{25}$$

For the parameters fixed in this paper ($\phi_0 = 0.4$, $K_1/K_0 = 0.9$), the limits are $V_1/V = 0.984$ (or 434 K_1-blocks out of 441), and $V_2/V = 0.01586$ (or 7 K_2-blocks out of 441). In this limit, $K_2/K_0 = 1.37 \times 10^7$ and $\widetilde{P}_{\text{peak}} = 466.12$.

Fig. 12 shows the effect of varying K_2/K_0 when ϕ_0 and K_1/K_0 are fixed. There is an optimal high permeability ($K_2/K_0 = 16.3$) where the overall flow resistance is minimal. Each point in Fig. 12 was obtained using the pressure gradient removal criterion. At each step, the block (or blocks) with the highest pressure gradient was chosen from among the blocks touching the K_2 region.

We continued in this direction, investigating the possibility of optimizing the low permeability, K_1/K_0. We found that it is possible to optimize both the low (K_1/K_0) and high (K_2/K_0) permeabilities. Fig. 13 shows the behavior of the overall resistance when K_2/K_0 has been optimized. The K_2-minimized overall resistance exhibits a minimum of

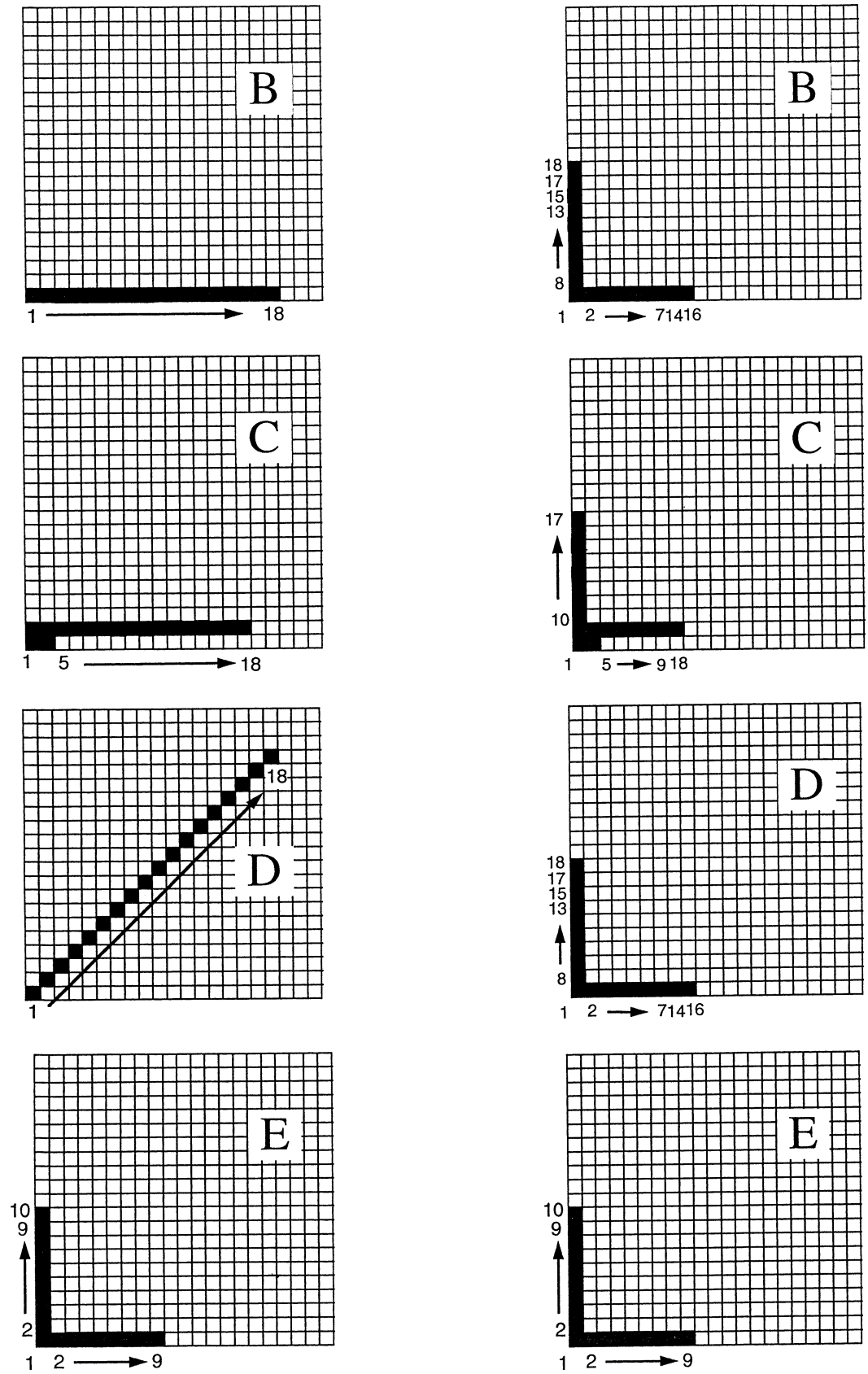

Fig. 11. Structures generated based on the pressure removal criterion (left) and the pressure gradient removal criterion (right).

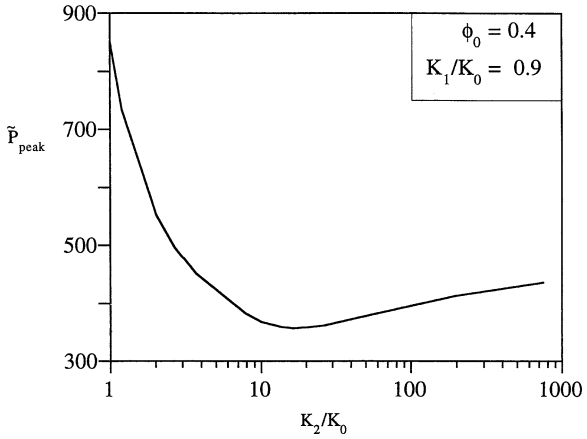

Fig. 12. The minimization of the overall flow resistance by selecting the high permeability of the finger shaped region.

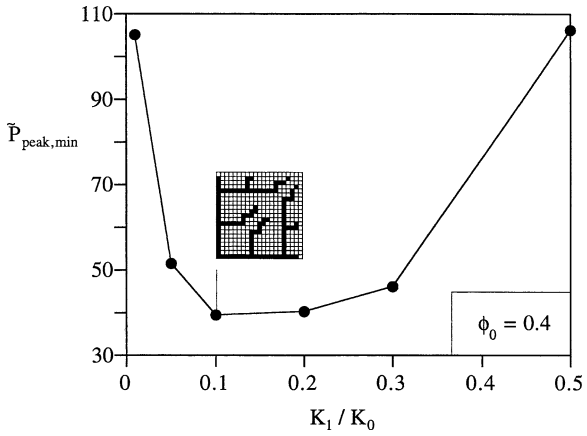

Fig. 13. The effect of the background (low) permeability on the overall flow resistance minimized in Fig. 12.

39.5 that corresponds to $K_2/K_0 = 993.1$ and $K_1/K_0 \approx 0.1$. Fig. 13 also shows the structure corresponding the optimal permeabilities, where $P_{\text{peak}} = 39.5$.

7. The medium responds to and attracts the flow

It is useful to look back and ask why dendritic flow structures occur in a flow between a point and an area, or a point and a volume. The answer is not the flow configuration, because there are many such flows where the pattern of streamlines is radial, without ramifications. It is "uniformly" distributed. For example, in a volumetrically averaged homogeneous and isotropic porous medium with a point source, the flow proceeds in straight lines away from the source. The same pattern is exhibited by thermal diffusion (heat conduction) from a heat source embedded in a homogeneous and isotropic medium. A source of electric current generates a similar pattern. Lines of constant pressure, temperature, and electric potential are circles with the source placed in the center (e.g., Fig. 8).

Unevenly distributed flows such as the tree-shaped networks occur because the originally homogeneous and isotropic medium has additional properties that are not evident until the flow process begins. First, the medium has a changing (malleable) constitution that allows it to organize itself into regions with distinct resistivities to flow—high and low resistivities. Second, a positive feedback (or economies of scale) mechanism is in place: the low resistivitiy becomes even lower when the flow rate that passes through the low-resistivity region increases. To see this, assume that instead of the two tubes with Hagen–Poisseuille flow (Fig. 1) we have two tubes filled with a thermally conductive solid. The thermal conductivity is constant, k. The overall temperature difference that drives the heat flow is ΔT. The conduction heat currents through the two tubes are

$$q_1 = \frac{\pi D_1^2 k \Delta T}{4L} \tag{26}$$

$$q_2 = \frac{\pi D_2^2 \Delta T}{4L} \tag{27}$$

The constraints are L and the total tube volume, namely $D_1^2 + D_2^2 = \text{constant}$. Because of this, the overall thermal conductance of the assembly is fixed,

$$(q_1 + q_2)\frac{4L}{\pi k \Delta T} = D_1^2 + D_2^2, \quad \text{constant} \tag{28}$$

Unlike in Fig. 1, there is no opportunity to optimize the structure (i.e., to select the size of D_1 vs. D_2), even though the heat flow configuration is analogous to the fluid flow arrangement. The difference, and the reason why in the case of fluid flow it is better when one large tube replaces two smaller ones, is visible when we compare Eqs. (1), (2) with Eqs. (25), (26). The fluid flow rates are proportional to D_1^4 and D_2^4, while the heat currents are proportional to D_1^2 and D_2^2. This means that fluid flow is analogous to heat conduction through a medium the conductivity of which increases with the tube diameter squared. The larger the stream through one tube, the lower the resistance, and this invites an even larger stream to flow through that tube. The medium responds to the flow, and, as a consequence of this property, develops itself into a macroscopically visible, unevenly distributed flow structure.

8. Concluding remarks

In this paper we documented the emergence of nonuniform flow structures when the objective is the minimization of the resistance to flow between one point and many points. The flow structure (flow path, channel sizes) was free to vary. In the first part of the paper, we modeled the flow as laminar fully developed through straight tubes. This allowed us to optimize flow paths between one point (source, or sink) and 3, 8, and 24 points positioned equidistantly in a square pattern in a plane. In the second part, we modeled the medium as a continuum with Darcy flow, where the flow structure is

the result of a process of erosion. Note that Hagen–Poiseuille flow is the analog of Darcy flow when the pore Reynolds number is considerably smaller than 10. In all the flows analyzed and optimized in this paper, the flow velocities were proportional to the local pressure gradients.

Several conclusions are worth stressing. Nonuniform, tree-shaped flow structures are the design solution to the minimization of global resistance to flow between a volume and one point. Channels are fewer and thicker near the tree root (source, sink). Eroded regions are wider near the tree root. The fluid flows along preferred paths. Flow maldistribution is necessary in the pursuit of lower flow resistance. Optimal maldistribution, or optimal distribution of imperfection (flow resistance) is the key to identifying the flow structure with minimal resistance. Conversely, the assumption of flow uniformity leads to designs with comparatively much higher resistances.

In the spaces bathed by flows through tubes with Hagen–Poiseuille flow, we saw that structural symmetry works in the direction of increasing the flow resistance. The minimization of resistance calls for the abandonment of flow symmetry, which is consistent with greater freedom in the design, and greater nonuniformity in the optimized structure.

For the erodable porous medium, the choice of different sizes and shapes of elemental blocks can be the subject of future research. Design and manufacture considerations will dictate the proper size and shape when the nonuniformity is man controlled (i.e., designed). The modeler criteria should dictate the proper size and shape in cases where the nonuniformity appears naturally (e.g., erosion) in a way that better captures the phenomena.

The flow structures developed in this paper illustrated the progress from simple structures (Fig. 2) to more complex structures (Fig. 6). In this direction, the tubes that connect the many points become a porous structure, one that has been *designed* to meet a global objective subject to global constraints. When the number of points with flow is infinite, as in the continuous medium with Darcy flow modeled in Fig. 7, the eroded flow structure starts from simple configurations and evolves toward more complex designs if the constraints allow it. Growth in size and complexity allows the flow structure to cover more effectively its designated space. The relative success of the maximum pressure gradient criterion (Fig. 10), which is more realistic as an erosion mechanism, lends additional support to the view that the maximization of flow access is a principle that accounts for structure in natural flows [10].

The mechanism that generates flow structures with minimal resistance, which served as focus for this study, is applicable in many fields where designed porous structures are needed. The trend for smaller and more compact heat-generating packages, which characterizes everything from heat exchangers to electronics, calls for flow structures that are effective in accessing all the points of a volume. In this direction of miniaturization and increased compactness and complexity, the flow systems themselves become designed porous media. To this end, search-acceleration techniques such as the identification of vanishing tubes (Table 3), are valuable tools for computer-aided design of optimally nonuniform flow structures in general. In future studies, it may be interesting to compare the results of the random searches with more elaborated multi-variable, nonlinear constrained optimization methods.

References

[1] I. Noda, D.G. Brownwest, C.C. Gryte, Effect of flow maldistribution on hollow fiber dialysis—Experimental studies, J. Membrane Sci. 5 (2) (1979) 209–225.
[2] P.R. Ponzi, L.A. Kaye, Effect of flow maldistribution on conversion and selectivity in radial flow fixed-bed reactors, AIChE J. 25 (1) (1979) 100–108.
[3] S.C. Kranc, The effect on nonuniform water distribution on cooling-tower performance, Energy 7 (6) (1983) 636–639.
[4] E. Tsotsas, On mass-transfer, dispersion, and macroscopic flow maldistribution in packed tubes, Chem. Engrg. Process 31 (3) (1992) 181–190.
[5] A. Leitao, P. Carlos, S. Santos, A. Rodrigues, Tracer experiments in fixed beds-effects of flow maldistribution on the estimation of transport kinetic-parameters, Chem. Engrg. J. Biochem. Engrg. J. 55 (3) (1994) 193–199.
[6] G.F. Jones, N. Lior, Flow distribution in manifolded solar collectors with negligible buoyancy effects, Sol. Energy 52 (3) (1994) 289–300.
[7] D. Bossan, J.M. Grillot, B. Thonon, S. Grandgeorge, Experimental-study of particulate fouling in an industrial plate heat-exchanger, J. Enhanced Heat Transfer 2 (1–2) (1995) 167–175.
[8] M.G. Beiler, D.G. Kroger, Thermal performance reduction in air-cooled heat exchangers due to nonuniform flow and temperature distribution, Heat Transfer Engrg. 17 (1) (1996) 82–92.
[9] C. Ranganayakulu, K.N. Seetharamu, The combined effects of wall longitudinal heat conduction and inlet fluid flow maldistribution in crossflow plate-fin heat exchangers, Heat Mass Transfer 36 (3) (2000) 247–256.
[10] A. Bejan, Shape and Structure, from Engineering to Nature, Cambridge University Press, Cambridge, 2000.
[11] A.M. Al Taweel, J. Militzer, J.M. Kan, F. Hamdullahpur, Motion of hydrodynamic aggregates, Powder Technology 50 (1989) 173–181.
[12] D. Tondeur, L. Luo, U. D'Ortona, Optimisation des transferts et des materiaux par l'approche constructale, Entropie 36 (2000) 32–37.
[13] M.-O. Coppens, G.F. Froment, The effectiveness of mass fractal catalysts, Fractals 5 (1997) 493–505.
[14] M.-O. Coppens, Y. Cheng, C.M. van den Bleek, Controlling fluidized bed operation using a novel hierarchical gas injection system, in: Paper 304d, AIChE Annual Meeting, Dallas, TX, October 31–November 5, 1999.
[15] M.-O. Coppens, Geometrical control of multiphase processes using a new fluid injection system, in: Paper 288c, AIChE Annual Meeting, Dallas, TX, October 31–November 5, 1999.
[16] M. Kearney, Control of fluid dynamics with engineered fractals—adsorption process applications, Chem. Engrg. Comm. 173 (1999) 43–52.
[17] D.V. Pence, Improved thermal efficiency and temperature uniformity using fractal-like branching channel networks, in: G.P. Celata, V.P. Carey, M. Groll, I. Tanasawa, G. Zummo (Eds.), Heat Transfer and Transport Phenomena, Begell House, New York, 2000, pp. 142–148.